development of positive charge in the transition state for these ligand substitution reactions. The increasing positive charge at the metal center during the breaking of the ruthenium-oxygen bond is destabilized by electron-withdrawing substituents, which therefore inhibits the dissociation of the aquo ligand. Thus, if ligand dissociation is the rate-determining step of the reaction, a corresponding reduction in the rate constant for ligand substitution for these complexes should be observed.

A plot of the $E_{1/2}$ values of the ruthenium(III/II) redox couples obtained for the aquo(phosphine)ruthenium(II) complexes in CH_2Cl_2 vs $\sum\sigma$ is also linear ($r^2 = 0.93$) and gave a ρ value of +0.10. The positive sign of the ρ value is consistent with the expectation that electron-donating groups stabilize, and electron-withdrawing groups destabilize, ruthenium(III), relative to the analogous unsubstituted complexes. The magnitude of ρ for this correlation indicates that the substituents on the phosphine ligands have a moderate effect on the resulting $E_{1/2}$ values, compared to other systems. Larger values of ρ have been obtained for the plot of $E_{1/2}$ against $\sum\sigma$ for III/II redox couples of ruthenium with acetylacetonate ($\rho = 0.38$–0.50)[88,89] and nitrosoarene ($\rho = 1.05$)[90] ligands. The ρ values obtained from a Hammett correlation with $E_{1/2}$ values for triazene 1-oxide complexes of ruthenium ($\rho = 0.10$–0.18)[91] closely match those found in this study. Finally, our observed ρ values are larger than those found for metal-centered redox reactions of substituted tetraphenylporphyrin complexes ($\rho = 0.02$–0.08),[92] where the ligand substituents are located further from the metal center and thus have a smaller effect on the $E_{1/2}$ values of the metal complexes.

Trialkylphosphine ligands were utilized in this study in order to investigate the role of the steric influence of the phosphine ligand on the aquo substitution kinetics. A plot of ln k vs ligand cone angle is given in Figure 4 and illustrates the linear rate constant enhancement promoted by the increasing phosphine ligand size. An increase in cone angle from 132 to 170° for the change from PEt_3 to PCy_3 corresponds to an increase in rate constant for ligand substitution by a factor of 750. This change is 3 times as large as the maximum variation in rate constants found for the substituted triphenylphosphine ligands, which suggests that the steric bulk of the coordinated phosphines has a much greater overall effect on the rate constant for aquo substitution for these complexes than the electronic properties of the phosphine ligands. These results are consistent with a dissociative type of mechanism, where the bulky cis-coordinated phosphine sterically destabilizes the ruthenium-aquo bond. The rate-controlling dissociation of the aquo ligand relieves the steric crowding at the metal center caused by the larger phosphine ligands and results in a corresponding increase in the rate of ligand substitution.

The activation parameters were determined for representative reactions involving the substitution of the aquo ligand by acetonitrile (Table III). The enthalpies and entropies of activation vary only over a small range, and as expected, the increase in the lability of the aquo ligand is followed by the lowering of the $\Delta H^{\ddagger}$ values for the corresponding reactions. The negative $\Delta S^{\ddagger}$ values found for these reactions in o-dichlorobenzene are consistent with negative activation entropies reported in previous studies of dissociative ligand substitution on ruthenium in nonaqueous solvents.[19] The negative values obtained for $\Delta S^{\ddagger}$ also suggest that the loss of the aquo ligand leads to a square-pyramidal type of five-coordinate intermediate in the transition state.[93] A positive value for $\Delta S^{\ddagger}$ would indicate the formation of a trigonal-bipyramidal intermediate in ligand substitution by the I_d mechanism on octahedral metal species.[93]

Acknowledgment. This work was supported in part by the donors of the Petroleum Research Fund, administered by the American Chemical Society, both the Biomedical Research Support Grant and the Research Development Fund of SUNY at Buffalo, and the ARCO Chemical Co. In addition, we gratefully acknowledge the contributions of Stephen A. Kubow to this paper, and R.A.L. acknowledges the award of an Allied Chemical Corp. fellowship.

(88) Patterson, G. S.; Holm, R. H. *Inorg. Chem.* **1972**, *11*, 2285–2288.
(89) (a) Endo, A. *Bull. Chem. Soc. Jpn.* **1983**, *56*, 2733–2738. (b) Endo, A.; Shimizu, K.; Sato, G. P. *Chem. Lett.* **1985**, 581–584.
(90) Bowden, W. L.; Little, W. F.; Meyer, T. J.; Salmon, D. *J. Am. Chem. Soc.* **1975**, *97*, 6897–6898.
(91) Mukherjee, R.; Chakravorty, A. *J. Chem. Soc., Dalton Trans.* **1983**, 955–959.
(92) (a) Kadish, K. M.; Morrison, M. M. *Inorg. Chem.* **1976**, *15*, 980. (b) Walker, F. A.; Beroiz, D.; Kadish, K. M. *J. Am. Chem. Soc.* **1976**, *98*, 3484. (c) Kadish, K. M.; Morrison, M. M.; Constant, L. A.; Dickens, L.; Davis, D. G. *J. Am. Chem. Soc.* **1976**, *98*, 8387.
(93) Tobe, M. L. *Inorg. Chem.* **1968**, *7*, 1260–1262.

Contribution from the Department of Chemistry, Purdue University, West Lafayette, Indiana 47907

Nickel(II) and Nickel(III) Bis(dipeptido) Complexes of α-Aminoisobutyric Acid

Sally L. Anliker, Mark W. Beach, Hsiupu D. Lee, and Dale W. Margerum*

Received December 1, 1987

Nickel(II) forms bis complexes with Aib_2 (the dipeptide of α-aminoisobutyric acid) that change from a high-spin form, $Ni^{II}(H_{-1}Aib_2)(Aib_2)^-$, to a low-spin form, $Ni^{II}(H_{-1}Aib_2)_2^{2-}$, with loss of a proton ($pK_a = 10.0$ at 25 °C) and the formation of a second N(peptide)–Ni(II) bond. Other dipeptides form tetragonally compressed six-coordinate bis complexes, but change of spin with pH is observed only when Aib is in the second residue. This is attributed to the electron-donating effect of the α-carbon methyl groups on the ligand field strength. A low-spin six-coordinate Ni(II) complex is proposed. Oxidation of the orange low-spin Ni(II) complex gives a dark olive green tetragonally compressed $Ni^{III}(H_{-1}Aib_2)_2^-$ complex that is very stable in neutral and basic solutions. The standard reduction potential for the Ni(III,II) couple is only 0.34 V (vs NHE). A self-exchange rate constant of 48 M^{-1} s^{-1} (25.0 °C, $I = 0.1$) is determined for $Ni^{III,II}(H_{-1}Aib_2)_2^{-,2-}$. This is 500 times larger than values found for outer-sphere electron-transfer reactions of Ni(III,II)–tripeptide complexes. Acid reacts with $Ni^{III}(H_{-1}Aib_2)_2^-$ in a three-step process to give two other Ni(III) complexes before decomposition to Ni(II) occurs. The last reaction ($k_{obsd} = 0.002$ s^{-1}) is independent of pH and is 100 times slower than the corresponding reaction of the bis(diglycinato)nickel(III) complex.

Introduction

Nickel(II) forms pale blue high-spin complexes in the presence of excess glycylglycine (GG). Potentiometric titrations[1,2] show that the predominant species at pH 11 is $Ni^{II}(H_{-1}G_2)_2^{2-}$, where H_{-1} refers to the number of deprotonated peptide nitrogens. This agrees with an X-ray crystal structure[3] for $Ni^{II}(H_{-1}G_2)_2^{2-}$ where Ni(II) is surrounded by two mutually perpendicular glycylglycine

(1) Kim, M. K.; Martell, A. E. *J. Am. Chem. Soc.* **1967**, *89*, 5138–5144.
(2) Kittl, W. S.; Rode, B. M. *Inorg. Chim. Acta* **1982**, *66*, 105–112.
(3) Freeman, H. C.; Guss, J. M. *Acta Crystallogr.* **1978**, *B34*, 2451–2458.

0020-1669/88/1327-3809$01.50/0

Scheme I

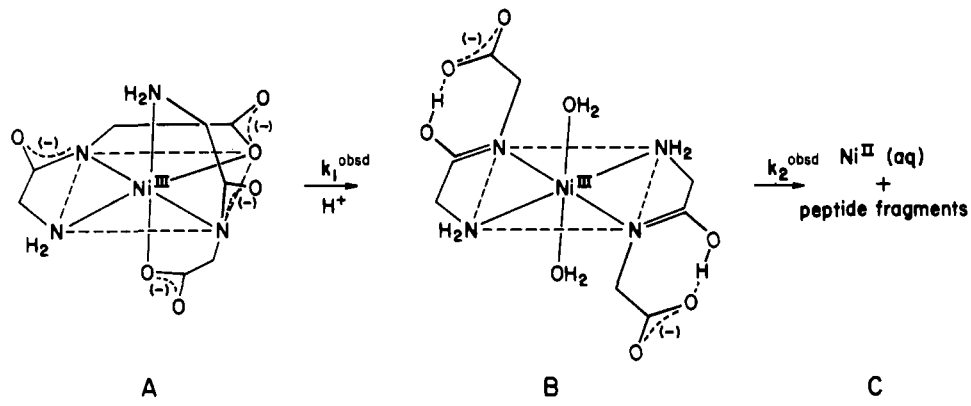

molecules that act as tridentate ligands via their amino, deprotonated peptide, and carboxylate groups (structure I). The

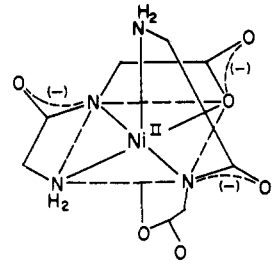

I

N^-–Ni–N^- axis is shorter than the other two axes, which places the Ni(II) in a tetragonally compressed octahedral environment. The bis(dipeptido)nickel(II) complexes with alanylalanine (AA), GA, AG, and α-aminoisobutyrylglycine (AibG) are also blue, high-spin complexes.[2,4] This behavior is in contrast to the Ni(II) complexes with tripeptides, tripeptide amides, and tetrapeptides, which are yellow, low spin, and square planar.[5]

In the present work Ni(II) complexes with excess Aib_2 (the dipeptide of α-aminoisobutyric acid) are examined. Blue high-spin bis(dipeptide) complexes once again form below pH 10, but above this pH an orange low-spin complex is formed with the stoichiometry $Ni^{II}(H_{-1}Aib_2)_2^{2-}$. Potentiometric, spectrophotometric, and magnetic data are used to characterize the orange Ni(II) species. It is readily oxidized to a Ni(III) bis(dipeptide) complex, which has an EPR spectrum that corresponds to a compressed-tetragonal six-coordinate structure. This Ni(III) complex is rapidly reduced back to the orange low-spin Ni(II) bis(dipeptide) form. The rapidly reversible redox behavior and the other properties of the nickel(II) complex indicate that $Ni^{II}(H_{-1}Aib_2)_2^{2-}$ has a low-spin six-coordinate compressed-tetragonal structure. Low-spin six-coordinate structures are unusual for nickel(II) complexes and are unique for nickel(II) peptide complexes.

Chemical or electrochemical oxidation of $Ni^{II}(H_{-1}G_2)_2^{2-}$ yields a black-violet tetragonally compressed octahedral Ni(III) bis complex, $Ni^{III}(H_{-1}G_2)_2^-$. This complex is stable in solution for several days at pH 7.5. The acid decomposition of the Ni(III) complex involves two sequential reactions[4] (Scheme I) in which the compressed Ni(III) complex (A) rearranges to a tetragonally elongated Ni(III) complex (B), which then undergoes self-redox to give Ni(II) plus dipeptide and oxidized peptide fragments. Oxidation of the $(Aib_2)_2$ complex gives an olive green $Ni^{III}(H_{-1}Aib_2)_2^-$ complex, which is stable indefinitely in neutral solution and is slow to decompose even in strong base. The complex decomposes in acid by a sequence of three reactions. The first two reactions give different Ni(III) complexes while the third reaction gives Ni(II). Aib residues in the dipeptide decrease the reactivity of the Ni(III) complex in acid. The relative rates of the self-redox decomposition of the bis(dipeptido)nickel(III) complexes decrease with GG > AG ≃ AibG > GA > AA >> Aib_2.

In recent years, a great deal of interest in Ni(III) complexes has been generated by the identification of Ni(III) in several hydrogenase[6-8] and carbon monoxide dehydrogenase[9] enzymes. These Ni(III) species exhibit amazing stability as well as low redox potentials (e.g., $E°$ = −0.145 V for the Ni(III) moiety in the hydrogenase from *Desulfovibrio gigas*),[10] and there is evidence that sulfur donors may be involved.[11,12]

The reduction potentials for mono(tripeptido)nickel(III) complexes are relatively high with $E°$ values (vs NHE) of 0.85 V for $Ni^{III}(H_{-2}G_3)$[13] and 0.83 V for $Ni^{III}(H_{-2}Aib_3)$.[14] The present work shows that the bis(dipeptido)nickelate(III) complexes have significantly lower potentials with $E°$ values of 0.66 V for $Ni^{III}(H_{-1}G_2)_2^{2-}$ and 0.34 V for $Ni^{III}(H_{-1}Aib_2)_2^-$. It is interesting that *C*-methyl substitution has little effect on the potentials of the mono(tripeptide) complexes but has a large effect on the potentials of the bis(dipeptide) complexes. As the $E°$ values decrease, the complexes become more stable in neutral and basic solution.

We find that the electron-transfer reactions of $Ni^{III}(H_{-1}Aib_2)_2^-$ are relatively rapid. Its reaction with $Cu^{II}(H_{-3}Aib_3a)^-$ (where Aib_3a is the tripeptideamide) is used to establish an outer-sphere self-exchange rate constant for the $Ni^{III,II}(H_{-1}Aib_2)_2^{-,2-}$ couple.

Experimental Section

Reagents. Carbobenzyloxyl (CBz) or benzyl ester (OBz) blocked amino acids were used to prepare the fully blocked dipeptides. CBzAib and AibOBz·TsOH, which are not commercially available, were prepared according to standard procedures for protecting amino acids.[15,16] $CBzAib_2OBz$ was prepared from CBzAib and AibOBz·TsOH by the mixed anhydride procedure of trimethylacetic acid.[17] The same proce-

(4) Jacobs, S. A.; Margerum, D. W. *Inorg. Chem.* **1984**, *23*, 1195–1201.
(5) Margerum, D. W.; Dukes, G. R. In *Metal Ions in Biological Systems*; Sigel, H., Ed.; Dekker: New York, 1974; Vol. 1, Chapter 5, pp 157–212.
(6) Kojima, N.; Fox, J. A.; Hausinger, R. P.; Daniels, L.; Orme-Johnson, W. H.; Walsh, C. *Proc. Natl. Acad. Sci. U.S.A.* **1983**, *80*, 378–382.
(7) Moura, J. J. G.; Moura, I.; Huynh, B. H.; Kruger, H. J.; Teixeira, M.; DuVarney, R. C.; DerVartanian, D. V.; Xavier, A. V.; Peck, H. D., Jr.; LeGall, J. *Biochem. Biophys. Res. Commun.* **1982**, *108*, 1388–1393.
(8) Albracht, S. P. J.; Graf, E. G.; Thauer, R. K. *FEBS Lett.* **1982**, *140*, 311–313.
(9) Ragsdale, S. W.; Ljungdahl, L. G.; DerVartanian, D. V. *Biochem. Biophys. Res. Commun.* **1983**, *115*, 658–665.
(10) Cammack, R.; Patil, D.; Aguirre, R.; Hatchikian, E. C. *FEBS Lett.* **1982**, *142*, 289–292.
(11) Scott, R. A.; Wallin, S. A.; Czechowski, M.; DerVartanian, D. V.; LeGall, J.; Peck, H. D., Jr.; Moura, I. *J. Am. Chem. Soc.* **1984**, *106*, 6864–6865.
(12) Lindahl, P. A.; Kojima, N.; Hausinger, R. P.; Fox, J. A.; Teo, B. K.; Walsh, C. T.; Orme-Johnson, W. H. *J. Am. Chem. Soc.* **1984**, *106*, 3062–3064.
(13) Bossu, F. P.; Margerum, D. W. *Inorg. Chem.* **1977**, *16*, 1210–1214.
(14) Murray, C. K.; Margerum, D. W. *Inorg. Chem.* **1983**, *22*, 463–469.
(15) Greenstein, J. P.; Winitz, M. *Chemistry of the Amino Acids*; Wiley: New York, 1961; Vol. 2.
(16) Stewart, J. M.; Yong, J. D. *Solid Phase Peptide Synthesis*, 2nd ed.; Pierce Chemical Co.: Rockford, II, 1984.
(17) Leplawy, M. T.; Jones, D. S.; Kenner, G. W.; Sheppartd, R. C. *Tetrahedron* **1960**, *11*, 39–51.

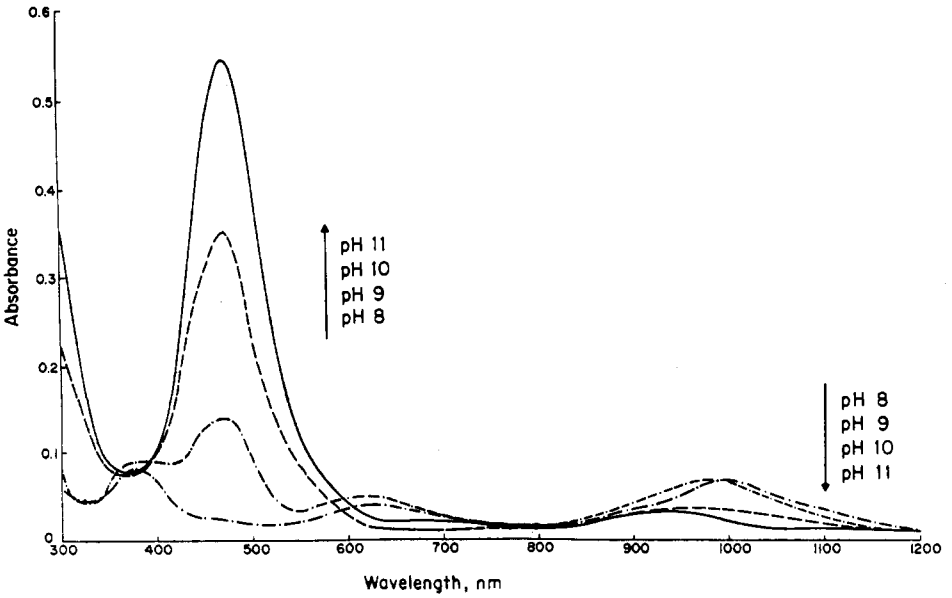

Figure 1. UV–visible–near-IR spectra of $Ni^{II}(Aib_2)_2$ (5.0×10^{-3} M) at 25 °C and I = 0.1 ($NaClO_4$), in a 1-cm cell.

dure was used to prepare CBzAibAOBz from CBzAib and AOBz·TsOH. CBzGAibOBz was prepared from CBzG and AibOBz·TsOH by the dicyclohexylcarbodiimide (DCC) method of amino acid coupling.[15,18] AAib was prepared by methods described previously.[18] Free dipeptides Aib_2, GAib, and AibA were prepared from their fully protected dipeptides by removing both protecting groups via hydrogenolysis over PdO in methanol and water (10:1 v/v).[15] Satisfactory elemental analyses were obtained for all dipeptides.

Anal. Calcd for Aib_2, $C_8H_{16}N_2O_3$: C, 51.04; H, 8.57; N, 14.89. Found: C, 50.98; H, 8.64; N, 14.76. Calcd for GAib·$^1/_2H_2O$, $C_6H_{12}N_2O_3 \cdot {}^1/_2H_2O$: C, 42.59; H, 7.74; N, 16.56. Found: C, 42.52; H, 7.67; N, 16.32. Calcd for AibA·$^1/_2H_2O$, $C_7H_{14}N_2O_3 \cdot {}^1/_2H_2O$: C, 45.89; H, 8.25; N, 15.29. Found: C, 45.78; H, 8.31; N, 15.10.

Nickel perchlorate was prepared from $NiCO_3$ and $HClO_4$ and was standardized by EDTA/murexide titration. The $Ni^{II}(Aib_2)_2$ complex was prepared by slow addition of NaOH to solutions containing $Ni(ClO_4)_2$ and a 10-fold excess of Aib_2.

$Ni^{III}(H_{-1}Aib_2)_2^-$ was prepared by oxidation of a solution of the Ni(II) complex at pH 11 in an electrochemical bulk flow cell.[14,19] Typical yields were about 60%. This species was observed to be somewhat sensitive to light and was kept in the dark. The $Ni^{III}(H_{-1}Aib_2)_2^-$ complex was separated from excess Aib_2 on a DEAE-Sephadex A-25 column (Pharmacia). A solution of 0.1 M NaCl was used as the mobile phase.

Solutions of hydroperoxyl anion (HO_2^-) were prepared by addition of NaOH to H_2O_2 (pK_a = 11.6).[20] Stock H_2O_2 solutions (Eastman Kodak 30% stabilizer free) were standardized by the method of Frew and coworkers.[21]

Solutions of $Cu^{II}(H_{-2}Aib_3)^-$ and $Cu^{II}(H_{-2}Aib_3a)$ for equilibrium and electron-transfer studies were prepared by addition of 0.1 N NaOH to solutions of $Cu^{II}(ClO_4)_2$ with 10% excess peptide or peptide amide. The syntheses of Aib_3[22] and Aib_3a[18] have been described previously.

Measurements. Electron paramagnetic resonance (EPR) spectra were obtained on a Varian E-109 X-band spectrophotometer modulated at 100 kHz and equipped with a Varian E-238 variable temperature cavity. Aqueous solutions for EPR were frozen at −150 °C and were magnetically dilute ([Ni(III)] < 1×10^{-3} M). The magnetic field was calibrated relative to α,α′-diphenyl-β-picrylhydrazyl (DPPH) which has a g value of 2.004. Splitting factors (g_{xx}, g_{yy}, and g_{zz}) and hyperfine coupling constants (a_{xx}, a_{yy}, and a_{zz}) were determined by a computer-generated spectral matching procedure.[23]

Acid decomposition and electron-transfer reactions of $Ni^{III}(H_{-1}Aib_2)_2^-$ were measured at 25.0 ± 0.1 °C with a Durrum stopped-flow spectrophotometer. Pseudo-first-order conditions were maintained for all reactions with Ni(III) as the limiting reagent and $HClO_4$ or buffer in at least 10-fold excess.

Ultraviolet–visible spectra and base decomposition data were recorded on a Perkin-Elmer 320 spectrophotometer interfaced to a Perkin-Elmer 3600 data station. Molar absorptivity (ε) values of Ni(III) complexes were determined by ascorbic acid titration. Near-IR data were recorded on a Cary 17 spectrophotometer.

Magnetic susceptibilities were measured by the Evans NMR method[24,25] with a Varian XL-200 NMR spectrometer. The frequency shifts of the water peak for solutions of $Ni^{II}(H_{-1}Aib_2)_2^{2-}$ were measured relative to pure water. These shifts can be related to effective magnetic moment (μ_{eff}) in μ_B.

HPLC analysis was accomplished by use of a Varian Model 5000 liquid chromatograph equipped with a Brownlee RP-300 Aquapore 10-μm column. The mobile phase was phosphate buffer (0.015 M, pH 2.2). UV detection at 210 nm was used, and quantitation was accomplished with a calibration curve for Aib_2 where peak areas were measured with a Hewlett-Packard 3390A integrator.

Hydrogen ion concentrations were measured with an Orion Research Model 701A pH meter equipped with either a Corning 476194 or a Sargent-Welch S 30072-15 combination glass electrode. The electrodes were calibrated at various ionic strengths (I) to correct the pH readings to −log [H^+] by means of perchloric acid-sodium hydroxide titrations. Stability constants for the Ni(II)–Aib_2 system were calculated from potentiometric titrations. The titrant, 0.1 N NaOH, was delivered from a calibrated Gilmont microliter syringe, No. S-4200. During the titration the solutions were kept under water-saturated argon to prevent absorption of CO_2. The ionic strength was maintained at 0.10 with $NaClO_4$ and all solutions were thermostated at 25.0 ± 0.1 °C. Titrations were performed with Aib_2:Ni ratios of 1:1, 2:1, and 3:1 from pH 2 to 8.2, 9.1, and 10.0, respectively. In all cases, precipitation was observed beyond this range and the titrations were discontinued. A modified version of the SCOGS computer program[18] was used to analyze the data. The standard deviation of titer was 1.6% and 1.8% for two 2:1 titrations and 1.2% for the 3:1 titration.

Results and Discussion

Nickel(II) Species. Figure 1 shows a series of electronic absorption spectra for the addition of base to a solution of $Ni(ClO_4)_2$ and excess Aib_2 as a function of pH. At pH 8, the solution is pale blue-green and has λ_{max} values of 380, 630, and 990 nm with molar absorptivities (ε) of 16, 8, and 10 M^{-1} cm^{-1}, respectively. This spectrum is typical of high spin, octahedral and tetragonally elongated octahedral Ni(II) complexes.[26] As the pH of the system is raised from 8 to 11, a 10-fold excess of ligand over the metal concentration is required to prevent nickel hydroxide precipitation. In addition, as the pH increases a higher intensity band appears

(18) Hamburg, A. W.; Nemeth, M. T.; Margerum, D. W. *Inorg. Chem.* **1983**, *22*, 3535–3541.
(19) Clark, B. R.; Evans, D. H. *J. Electroanal. Chem. Interfacial Electrochem.* **1976**, *69*, 181–184.
(20) Everett, A. J.; Minkoff, G. J. *Trans. Faraday Soc.* **1953**, *49*, 410–414.
(21) Frew, J. E.; Jones, P.; Sholes, G. *Anal. Chim. Acta* **1983**, *155*, 139–150.
(22) Kirksey, S. T., Jr.; Neubecker, T. A.; Margerum, D. W. *J. Am. Chem. Soc.* **1979**, *101*, 1631–1633.
(23) Toy, A. D.; Chaston, S. H. H.; Pilbrow, J. R.; Smith, T. D. *Inorg. Chem.* **1971**, *10*, 2219–2225.
(24) Deutsch, J. L.; Poling, S. M. *J. Chem. Educ.* **1969**, *46*, 167–168.
(25) Evans, D. F. *J. Chem. Soc.* **1959**, 2003–2005.
(26) Lever, A. B. P. *Inorganic Electronic Spectroscopy*; Elsevier: Amsterdam, 1984; p 507.

Table I. Cumulative Association Constants[a] and Representative Equilibrium Constants for Nickel(II) Dipeptide Complexes

dipeptide	log β_{101}	log β_{102}	log β_{1-12}	log β_{1-22}	pK_{1-}[b]	pK_{2-}[c]	ref
G_2	4.08	7.32	−1.8	−11.57	9.1	9.8	*d*
GA	4.23	7.60	−1.5	−12.19	9.1	10.7	*e*
AG	3.60	6.41	−2.2	−12.08	8.6	9.9	*d*
LG	3.39	6.21	−2.4	−12.31	8.6	9.9	*d*
A_2	3.65	6.57	−2.4	−12.31	9.0	9.9	*d*
V_2	3.12	5.94	−3.1	−12.41	9.0	9.3	*e*
Aib_2	3.51 (3)	6.24 (3)	−3.5 (1)	−13.45 (6)	9.7	10.0	*f, g*

[a] Defined in eq 1. [b] pK_{1-} = log β_{102} − log β_{1-12}; for K_{1-}, $NiL_2 \rightleftarrows Ni(H_{-1}L)L^- + H^+$. [c] pK_{2-} = log β_{1-12} − log β_{1-22}; for K_{2-}, $Ni(H_{-1}L)L^- \rightleftarrows Ni(H_{-1}L)_2^{2-} + H^+$. [d] Reference 2; I = 0.20 M KCl, 20 °C. [e] Reference 27; I = 0.10 M KNO_3, 25 °C. [f] This work; I = 0.10 M $NaClO_4$, 25.0 ± 0.1 °C. Uncertainties are 1 standard deviation in the last digit. [g] pK_a values for Aib_2: pK_{COOH} = 3.67; pK_{NH} = 8.26.[18]

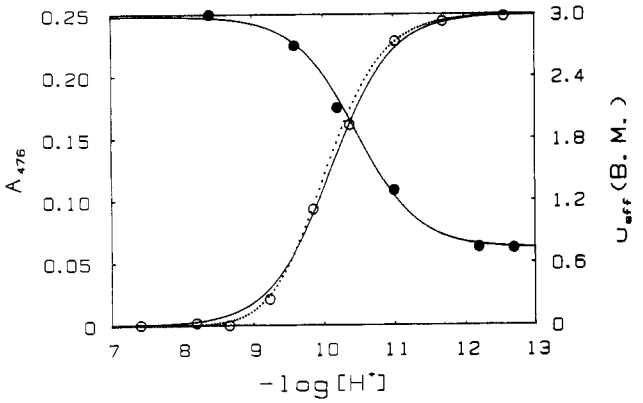

Figure 2. Absorbance data at 476 nm (○) and magnetic moment data (●) for $Ni^{II}(Aib_2)$ with 10:1 Aib_2:nickel ratio at 25 °C and I = 0.05.

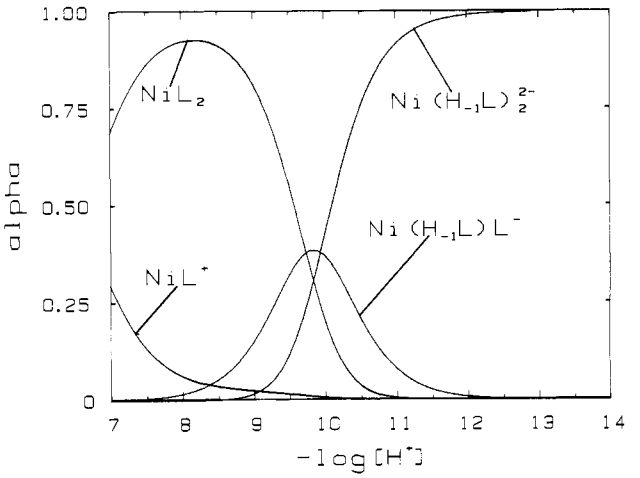

Figure 3. Speciation diagram of the potentiometric data for the Ni(II)–Aib_2 system with a 10:1 metal-to-ligand ratio at I = 0.1 ($NaClO_4$).

in the visible region and the near-IR band at 990 nm decreases in intensity. At pH 11, a single peak is evident in the visible region at 476 nm with an ϵ value of 110 M^{-1} cm^{-1}. This spectrum is typical of low-spin nickel(II) complexes.[26] The change from high-spin to low-spin is reversible with pH. Low-spin Ni(II) complexes usually have a square-planar geometry, but we do not believe that is the case in this instance.

Magnetic and spectrophotometric measurements in the pH range 7–13 used a 10-fold excess of Aib_2 in order to prevent $Ni(OH)_2$ formation at the high pH values. Magnetic susceptibility measurements show that μ_{eff} changes as a function of solution acidity and the solid line in Figure 2 is the calculated curve for a single-proton deprotonation. The μ_{eff} values level off at 0.74 μ_B rather than zero, the expected value for a diamagnetic complex. Absorbance measurements for this system at 476 nm are also plotted in Figure 2. Again, the solid line shows the calculated one-proton curve. Clearly, a single deprotonation occurs at pH 9–11 that involves the conversion of Ni(II) from a high-spin state to a low-spin species. The fit in the pH range 7–9 is poorer than at pH 9–11. This implies that additional processes occur in this range. The calculated pK_a values for the one proton process are 10.5 and 10.1 for the magnetic and spectrophotometric data, respectively.

Potentiometric titrations were performed on this system with 1:1, 2:1, and 3:1 Aib_2:Ni ratios. The generalized cumulative formation reaction of dipeptide ligands is given in eq 1. Com-

$$mNi^{2+} + hH^+ + lL \xrightleftharpoons{\beta_{mhl}} Ni_m(H_hL_l) \qquad (1)$$

putations based on the following species were used to fit the potentiometric data: Ni^{2+}, NiL^+, NiL_2, $Ni(H_{-1}L)L^-$, and $Ni(H_{-1}L)_2^{2-}$, where L = $H_2NC(CH_3)_2CONHC(CH_3)_2CO_2^-$. Similar species have been proposed for Ni(II) complexes with other dipeptides such as GA[2,27] and GG.[2,28] A NiL_3^- species is not included, although this species has been proposed for other nickel(II) dipeptide systems, because the calculated fit of the potentiometric data (standard deviation of titer) is not improved by including this species. (Steric hindrance probably prevents formation of the tris complex.) An alternative model that includes $Ni(H_{-1}L)$ rather than $Ni(H_{-1}L)L^-$ also fits the potentiometric data but does not explain the one-proton process observed in the magnetic and spectrophotometric data. In addition, the calculations show that the concentration of $Ni(H_{-1}L)$ formed is negligible at high ligand-to-metal ratios. The combination of the magnetic, spectrophotometric, and potentiometric data indicate that the reaction in eq 2 occurs in the pH range 9–11. The

$$Ni(H_{-1}L)L^- \rightleftarrows Ni(H_{-1}L)_2^{2-} + H^+ \qquad (2)$$

speciation diagram based on this model at an Aib_2:Ni ratio of 10:1 is shown in Figure 3, where α is the fraction of Ni(II) present in the various complexes. The calculated pK_a value for the reaction in eq 2 is 10.0 from the potentiometric analysis (pK_{2-} in Table I), which compares well with the values determined from magnetic and spectrophotometric titrations. The dotted line in Figure 2 gives the absorbance curve calculated by use of the pK_a values from the potentiometric data (pK_{1-} = 9.7 and pK_{2-} = 10.0). These calculations are based on an ϵ value of 125 M^{-1} cm^{-1} for $Ni^{II}(H_{-1}Aib_2)_2^{2-}$ at 476 nm and pH 13 and an ϵ value of zero for all other species under these conditions. As expected, this curve provides a better fit to the absorbance data than the simple one-proton model (solid line). The use of these pK_a values does not improve the fit of the magnetic data; however, the measured NMR frequency shifts are small, and these data are less precise than the potentiometric or spectrophotometric data.

The stability constants for the $Ni^{II}Aib_2$ system as well as those from other Ni(II)–dipeptide titrations are shown in Table I. Aib_2 forms less stable Ni(II) species, relative to the Ni(II) complexes with other dipeptides, as evidenced by lower stability constants for most of the Aib_2 species in Table I. This explains the precipitation problems experienced in preparing the $Ni^{II}(H_{-1}Aib_2)_2^{2-}$ complex. Interference from $Ni(OH)_2$ prevented the growth of crystals for X-ray structure analysis.

The proposed structures are shown in Scheme II, where R = CH_3. The structure for $Ni^{II}Aib_2^+$ (**1**) is based on the proposed structure for $Ni^{II}GG^+$.[28] The proposed structure for $Ni^{II}(Aib_2)_2$ (**2**) has Aib_2 residues coordinated in a mutually perpendicular

(27) Brookes, G.; Pettit, L. D. *J. Chem. Soc., Dalton Trans.* **1975**, 2106–2112.
(28) Kaneda, A.; Martell, A. E. *J. Coord. Chem.* **1975**, *4*, 137–151.

Scheme II

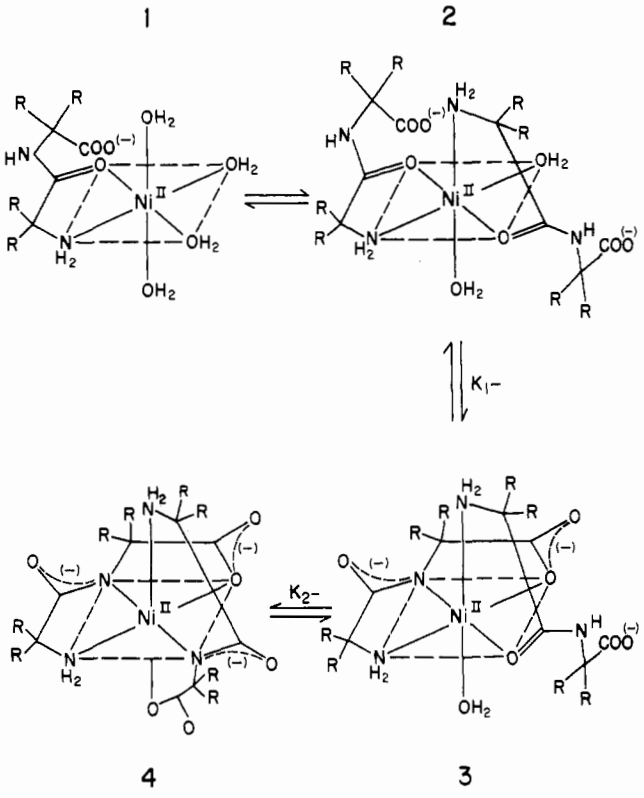

arrangement with carbonyl groups occupying two equatorial sites. The $Ni^{II}(Aib_2)_2$ complex is the predominant species at pH 8 and undergoes two sequential peptide nitrogen deprotonations to give $Ni^{II}(H_{-1}Aib_2)Aib_2^-$ (**3**) and $Ni^{II}(H_{-1}Aib_2)_2^{2-}$ (**4**). From the magnetic susceptibility data, both $Ni^{II}(Aib_2)_2$ and $Ni^{II}(H_{-1}Aib_2)Aib_2^-$ are high-spin complexes whereas $Ni^{II}(H_{-1}Aib_2)_2^{2-}$ is predominantly low-spin (Figure 2). However, the effective magnetic moment does not reach a value of zero (completely low-spin) at pH greater than 11. Rather, μ_{eff} remains at 0.74 μ_B above pH 12.

Several nickel(II) systems have been studied that exhibit anomalous magnetic moments in solution or in the melt. Behavior of this type has been attributed to the formation of six-coordinate species by the addition of two polar solvent molecules[29-31] or to square-planar/tetrahedral equilibria in inert solvents.[32-34] $Ni(etu)_4I_2$ (etu = ethylenethiourea)[35] and $Ni(MImt)_4(ClO_4)_2$ (MImt = 1-methylimidazoline-2-thione)[36] are described as diamagnetic and six-coordinate complexes. However, the I^- and ClO_4^- bond distances are 3.2 and 3.6 Å, respectively. Lever[26] states that six-coordinate low-spin tetragonal complexes are virtually unknown.

The UV–vis spectrum of $Ni^{II}(H_{-1}Aib)_2^{2-}$ at pH 11 is typical of low-spin Ni(II) complexes except for a very small near-IR band at 990 nm ($\epsilon < 2$ M^{-1} cm^{-1}). Magnetic data indicate that the complex is 60% low spin at pH 11. By comparison of the UV–vis spectra, $Ni^{II}(H_{-1}AAib)_2^{2-}$ is approximately 50% low spin at pH 11, while $Ni^{II}(H_{-1}GAib)_2^{2-}$ is only about 10% low spin at pH 11. In contrast, the observed magnetic moment for the bis(diglycine) complex is 3.0 μ_B at pH 11, which falls in the range of μ_{eff} values generally accepted for octahedral nickel(II) (2.80–3.40 μ_B).[35] The

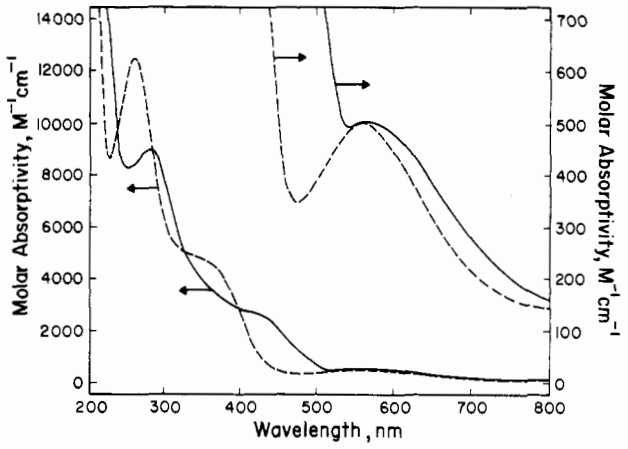

Figure 4. UV–visible spectra of Ni(III) bis(dipeptide) complexes: (–) $Ni^{III}(H_{-1}Aib_2)_2^-$; (---) $Ni^{III}(H_{-1}G_2)_2^-$.

Ni(II) complexes with GA, AG, AA, AibG, and AibA are also high-spin octahedral at high pH. However, the nickel(II) bis(dipeptide) complexes with Aib in the second peptide residue exhibit high-spin/low-spin equilibria when both peptide nitrogens are deprotonated. The proposed structure for $Ni^{II}(H_{-1}Aib_2)_2^{2-}$ (**4** in Scheme II) has two deprotonated peptide nitrogens with the Aib_2 ligands coordinated in a mutually perpendicular arrangement. This structure is analogous to that of $Ni^{II}(H_{-1}G_2)_2^{2-}$, which was determined by X-ray crystallography.[3] An explanation for the high-spin/low-spin equilibrium in the case of $Ni^{II}(H_{-1}Aib_2)_2^{2-}$ is that the electron-donating effect of the α-carbon methyl substituents causes the donor strength of the peptide nitrogens to increase upon deprotonation. This enhances the splitting of the energy levels in the compressed-tetragonal structure sufficiently to favor the formation of a low-spin species. It explains why only dipeptides with Aib in the second residue exhibit the spin pairing. However, the degree of spin pairing also increases as the first residue is changed from G to A to Aib. The μ_{eff} value of 0.74 μ_B for $Ni^{II}(H_{-1}Aib_2)_2^{2-}$ indicates the complex is about 75% low spin and 25% high spin above pH 12. We suggest that these two states are in rapid equilibrium and have similar structures.

There are several reasons why we believe that low-spin $Ni^{II}(H_{-1}Aib_2)_2^{2-}$ is a tetragonally compressed six-coordinate complex and is not a square-planar complex. (1) Its potentiometric behavior parallels that of the six-coordinate $(G_2)_2$ complex. (2) A square-planar arrangement (with four nitrogens in a plane) would cause steric hindrance that is not present when the two Aib_2 ligands are mutually perpendicular. (3) The $Ni^{II}(H_{-1}Aib_2)_2^{2-}$ complex is rapidly oxidized to a stable tetragonally compressed six-coordinate $Ni^{III}(H_{-1}Aib_2)_2^-$ complex, which in turn can be rapidly reduced back to the initial low-spin Ni(II) form. (4) If the Ni(II) complex had a square-planar arrangement, then its oxidation would be expected to give a tetragonally elongated Ni(III) complex with two axially coordinated water molecules as is observed with tripeptide, tetrapeptide, and tripeptide amide complexes.[13,37,38] This does not occur, although the tetragonally compressed Ni(III) complex will react with acid (pH <4) to give a tetragonally elongated Ni(III) complex. (5) A tetragonally compressed six-coordinate Ni(II) complex should become low spin when the splitting of the energy levels between the $d_{x^2-y^2}$ and d_{z^2} orbitals is large.

Nickel(III) Species. The $Ni^{II}(H_{-1}Aib_2)_2^{2-}$ complex at pH 11 (primarily low spin) can be electrochemically or chemically oxidized to a dark olive green paramagnetic species. This complex has ultraviolet–visible absorption bands at 270, 410 (shoulder), and 550 nm (shoulder) with molar absorptivities of 9000, 2700, and 500 M^{-1} cm^{-1}, respectively. The UV–vis spectrum for the complex, which is assumed to be $Ni^{III}(H_{-1}Aib_2)_2^-$, and the

(29) Wilkins, R. G.; Yelin, R.; Margerum, D. W.; Weatherburn, D. C. *J. Am. Chem. Soc.* **1969**, *91*, 4326.
(30) Basolo, F.; Matoush, W. R. *J. Am. Chem. Soc.* **1953**, *75*, 5663–5666.
(31) Clark, H. C.; Odell, A. L. *J. Chem. Soc.* **1955**, 3431–3435.
(32) Pignolet, L. H.; Horrocks, W. D., Jr.; Holm, R. H. *J. Am. Chem. Soc.* **1970**, *92*, 1855–1863.
(33) Holm, R. H.; Swaminathan, K. *Inorg. Chem.* **1963**, *2*, 181–186.
(34) Eaton, D. R.; Phillips, W. D.; Caldwell, D. J. *J. Am. Chem. Soc.* **1963**, *85*, 397–406.
(35) Holt, S. L., Jr.; Carlin, R. L. *J. Am. Chem. Soc.* **1964**, *86*, 3017–3024.
(36) O'Neill, M. E.; Raper, E. S.; Nowell, I. W.; Daniels, J. A. *Inorg. Chim. Acta* **1981**, *54*, L243–L247.
(37) Lappin, A. G.; Murray, C. K.; Margerum, D. W. *Inorg. Chem.* **1978**, *17*, 1630–1634.
(38) Subak, E. J., Jr.; Loyola, V. M.; Margerum, D. W. *Inorg. Chem.* **1985**, *24*, 4350–4356.

Scheme III

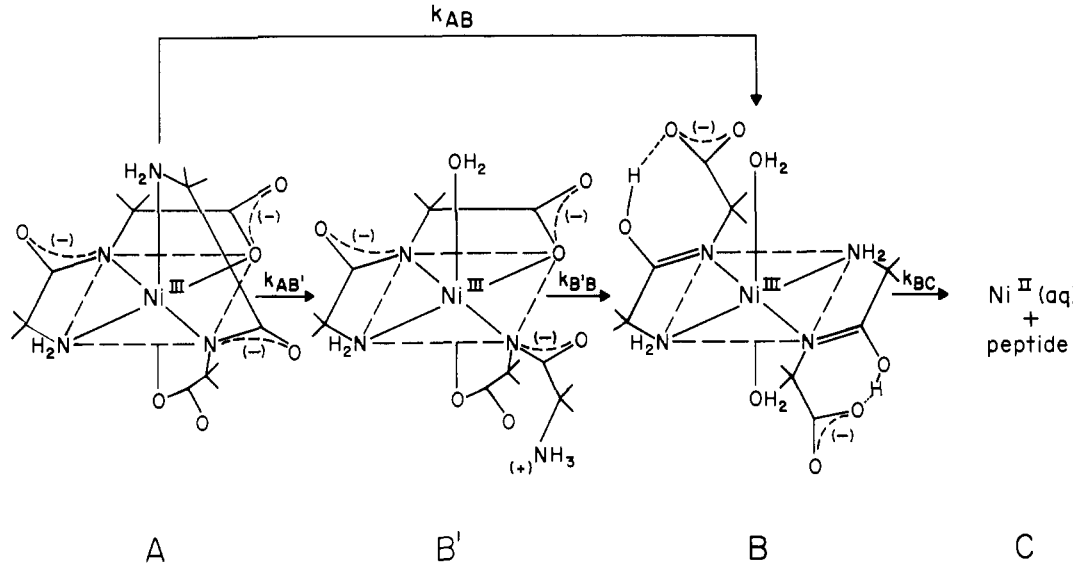

Table II. Calculated EPR Parameters for $Ni^{III}(H_{-1}Aib_2)_2^-$ (A) and Its Acid Decomposition Intermediates (B′ and B)

species	g_{xx}	g_{yy}	g_{zz}	w_{xx}	w_{yy}	w_{zz}	a_{xx}	a_{yy}	a_{zz}
A	2.076	2.063	2.218	17.0	9.0	17.0	20	15	1
B′	2.225	2.192	2.015	13.0	16.0	5.0	1	1	1
B	2.245	2.233	2.017	21.0	15.0	5.0	1	1	1

spectrum for $Ni^{III}(H_{-1}G_2)_2^-$ are shown in Figure 4. $Ni^{III}(H_{-1}G_2)_2^-$ is violet-black in color and has λ_{max} (ϵ, M^{-1} cm^{-1}) values of 255 (12000), 355 (5000) and 560 (500) nm.[4] The shift in the charge-transfer bands to longer wavelengths for $Ni^{III}(H_{-1}Aib_2)_2^-$ results in the deep olive green color rather than the violet-black of the diglycine complex. The $Ni^{III}(H_{-1}Aib_2)_2^-$ complex is rapidly reduced to the orange low-spin $Ni^{II}(H_{-1}Aib_2)_2^{2-}$ complex with the hydroperoxyl anion ($E°(O_2/HO_2^-)$ = 0.022 V (vs NHE) in 1 M base).[39] The second-order rate constant for the reaction in eq 3 (k_{12}) is 4.26 ± 0.06 M^{-1} s^{-1} in 0.50 M NaOH at 25.0 °C.

$$2Ni^{III}(H_{-1}Aib_2)_2^- + HO_2^- + OH^- \xrightarrow{k_{12}} 2Ni^{II}(H_{-1}Aib_2)_2^{2-} + O_2 + H_2O \quad (3)$$

In 1 M NaOH, $Ni^{III}(H_{-1}Aib_2)_2^-$ has a half-life of about 20 h, and it is indefinitely stable at pH 8–12 at room temperature when protected from light. The electron paramagnetic resonance spectrum for this complex (Figure 5) shows $g_{\parallel} > g_{\perp}$, in contrast to typical EPR spectra of Ni(III) tripeptide complexes with a tetragonally elongated octahedral geometry where $g_{\perp} > g_{\parallel}$. The parameters for the calculated spectrum in Figure 5 are given in Table II (species A) where w_{xx}, w_{yy}, and w_{zz} are broadening parameters and a_{xx}, a_{yy}, and a_{zz} are hyperfine coupling constants. This spectrum is similar to the EPR spectrum for $Ni^{III}(H_{-1}G_2)_2^-$.[4] A tetragonally distorted octahedral geometry has been proposed for $Ni^{III}(H_{-1}G_2)_2^-$ where the N^-–Ni^{3+}–N^- axis is compressed relative to the other two axes. An analogous structure (A in Scheme III) is proposed for the olive green Ni(III) complex with Aib_2 residues coordinated in a mutually perpendicular arrangement. This 2:1 Aib_2:Ni(III) stoichiometry was confirmed by separating the Ni(III) complex from excess Aib_2 chromatographically on a DEAE–Sephadex column. The Ni(III) complex was quantitated in the eluent by the UV–vis absorbance at 410 nm. The Aib_2 content was determined by HPLC analysis under acidic conditions that cause dissociation of Aib_2 from the metal. This analysis yields an Aib_2:Ni(III) ratio of 1.92 ± 0.04.

Reduction Potential Measurements. Cyclic voltammograms for the Ni(III)–Ni(II)–$(Aib_2)_2$ couple on carbon-paste and glassy-carbon electrodes give an apparent $E_{1/2}$ of 0.85 V (vs NHE); however, the voltammograms show pseudoreversible behavior (E_{p-p} = 90–210 mV for pH 9–13). In addition, peak current is directly proportional to scan rate, which indicates that the complex is adsorbing on the electrode surface. However, $Ni^{II}(H_{-1}Aib_2)_2^{2-}$ is readily oxidized by $Cu^{III}(H_{-3}G_2AibG)^-$ ($E°$ = 0.52 V vs NHE),[40] which indicates that the $E°$ for $Ni^{III,II}(H_{-1}Aib_2)_2^{-,2-}$ is less than 0.52 V.

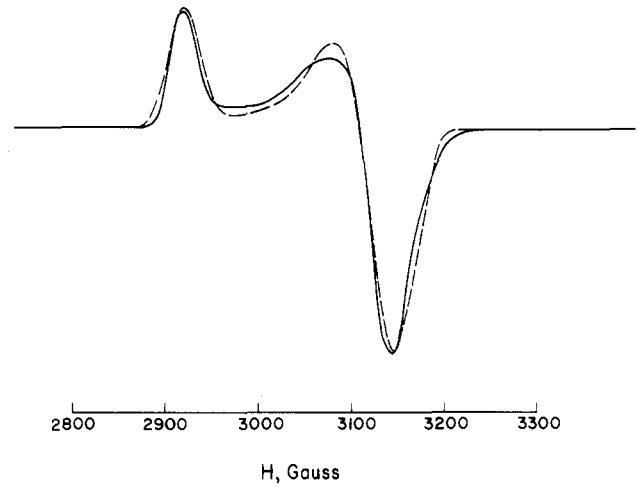

Figure 5. EPR spectrum for $Ni^{III}(H_{-1}Aib_2)_2^-$ at pH 9, −150 °C, at I = 0.1 $NaClO_4$) (—) experimental curve; (- - -) calculated curve.

The equilibrium constant for the reaction of $Ni^{III}(H_{-1}Aib_2)_2^-$ with $Cu^{II}(H_{-3}Aib_3a)^-$ (eq 4) (where Aib_3a is the amide of the Aib tripeptide) was measured spectrophotometrically in 1 M NaOH. At this base concentration, an additional equilibrium exists between $Cu^{III}(H_{-3}Aib_3a)$ and its amine-deprotonated form, $Cu^{III}(H_{-4}Aib_3a)^-$ (pK_a = 12.5),[41] as indicated in eq 5. Absorbance values of equilibrium mixtures of $Cu^{II}(H_{-3}Aib_3a)^-$, $Cu^{III}(H_{-4}Aib_3a)^-$, $Ni^{II}(H_{-1}Aib_2)^{2-}$, and $Ni^{III}(H_{-1}Aib_2)_2^-$ were measured at 550 nm where the molar absorptivities are 30, 1500, 20, and 500 M^{-1} cm^{-1}, respectively. Initial concentrations of Cu^{II}-

$$Cu^{II}(H_{-3}Aib_3a)^- + Ni^{III}(H_{-1}Aib_2)_2^- \overset{K_e}{\rightleftharpoons} Cu^{III}(H_{-3}Aib_3a) + Ni^{II}(H_{-1}Aib_2)_2^{2-} \quad (4)$$

$$Cu^{III}(H_{-3}Aib_3a) \overset{K_a}{\rightleftharpoons} Cu^{III}(H_{-4}Aib_3a)^- + H^+ \quad (5)$$

(39) Sawyer, D. T.; Nanni, E. J., Jr. In *Oxygen and Oxy-Radicals in Chemistry and Biology*; Rodgers, M. A. J., Powers, E. L., Eds.; Academic: New York, 1981; p 17.

(40) Hamburg, A. W. Ph.D. Thesis, Purdue University, 1982.

(41) Hinton, J. P.; Margerum, D. W. *Inorg. Chem.* **1986**, *25*, 3248–3256.

Table III. Kinetic Data for the Electron Transfer Reaction of $Ni^{III}(H_{-1}Aib_2)_2^-$ with $Cu^{II}(H_{-3}Aib_3a)^-$

$[Cu^{II}(H_{-3}Aib_3a)^-]$, M	k(obsd),[a] s^{-1}	ref
2.55×10^{-3}	1.81 ± 0.05	*b*
2.65×10^{-3}	2.21×0.05	*c*
5.10×10^{-3}	4.22×0.03	*b*
5.50×10^{-3}	4.70 ± 0.05	*c*
7.80×10^{-3}	6.5 ± 0.2	*b*
8.55×10^{-3}	7.1×0.1	*c*
1.06×10^{-2}	8.3 ± 0.8	*b*
1.13×10^{-2}	9.7 ± 0.5	*c*

[a] Values are the average of at least three trials. Uncertainties are 1 sample standard deviation. [b] −log $[H^+]$ = 12.0; phosphate buffer; I = 0.1; $[Ni(III)] = 2.4 \times 10^{-4}$ M; 25.0 °C. [c] 0.1 M NaOH; I = 0.1; $[Ni(III)] = 2.2 \times 10^{-4}$ M; 25.0 °C.

$(H_{-3}Aib_3a)^-$ and $Ni^{III}(H_{-1}Aib_2)_2^-$ for this study were 1×10^{-4} and 1×10^{-3} M, respectively. For $K_w = 10^{-13.8}$ (I = 1.0), a value of 0.26 is obtained for K_e. This equilibrium constant and the known reduction potential for the copper couple in eq 4 (0.37 V vs NHE)[42] give a reduction potential of 0.34 V (vs NHE) for the $Ni^{III,II}(H_{-1}Aib_2)_2^{-,2-}$ couple. This reduction potential is considerably lower than those of the mono(tripeptide) and tetrapeptide Ni(III,II) couples (0.79–0.96 V).[13]

The reduction potential for $Ni^{III}(H_{-1}G_2)_2^-$ was previously estimated to be between 0.66 and 0.83 V (vs NHE).[4] A more precise value for this potential was obtained spectrophotometrically by measuring the extent of the equilibrium in eq 6 at 395 nm and

$$Ni^{III}(H_{-1}G_2)_2^- + Cu^{II}(H_{-2}Aib_3)^- \overset{K_e}{\rightleftharpoons} Ni^{II}(H_{-1}G_2)^{2-} + Cu^{III}(H_{-2}Aib_3) \quad (6)$$

−log $[H^+]$ = 10.8. Molar absorptivities at 395 nm for $Ni^{III}(H_{-1}G_2)_2^-$ and $Cu^{III}(H_{-2}Aib_3)$ are 3400 and 5200 M^{-1} cm^{-1}, respectively. At pH 10.8, $Ni^{II}(H_{-1}G_2)_2^{2-}$ is the main form of bis(diglycinato)nickel(II) in solution since the pK_a value is 9.77 for the reaction in eq 7 and the extent of amine deprotonation of

$$Ni^{II}(H_{-1}G_2)_2(G_2)^- \overset{K_a}{\rightleftharpoons} Ni^{II}(H_{-1}G_2)_2^{2-} + H^+ \quad (7)$$

$Cu^{III}(H_{-2}Aib_3)$ is small (pK_a = 11.8).[43] A redox potential for the nickel couple of 0.66 V was obtained by using the experimental value of K_e and the known value of $E°$ = 0.66 V (vs NHE)[22] for the copper couple. Thus, the redox potential for $Ni^{III}(H_{-1}Aib_2)_2^-$ is 0.32 V less than the $E°$ for the corresponding bis(diglycinato)nickel(III) complex. This reflects the unusual stability of $Ni^{III}(H_{-1}Aib_2)_2^-$ as well as the relative instability of $Ni^{II}(H_{-1}Aib_2)_2^{2-}$.

Electron-Transfer Reactions. The rate of the electron-transfer cross-reaction between $Ni^{III}(H_{-1}Aib_2)_2^-$ and excess $Cu^{II}(H_{-3}Aib_3a)^-$ was studied in the pH range 12–13. Excellent pseudo-first-order behavior was found (Table III), and the observed first-order rate constants depended on the Cu(II) concentration (Figure 6). Thus, the reaction follows the simple rate relationship given in eq 8. The

$$\text{rate} = k_{12}[Ni^{III}(H_{-1}Aib_2)_2^-][Cu^{II}(H_{-3}Aib_3a)^-] \quad (8)$$

second-order electron transfer rate constant, k_{12}, is 830 ± 13 M^{-1} s^{-1}. This reaction is predicted to be a simple outer-sphere electron transfer because the Ni(III) complex is coordinatively saturated and would not be expected to break a metal–peptide bond in order to allow a solvent molecule to bridge the Cu(II) and Ni(III) centers.

An estimate for the self-exchange rate of the $Ni^{III,II}(H_{-1}Aib_2)_2^{-,2-}$ couple is obtained by applying the Marcus correlation,[44] eq 9 and 10, where k_{22} is the rate of self-exchange for

$$k_{12} = (k_{11}k_{22}K_{12}f)^{1/2} \quad (9)$$

$$\log f = (\log K_{12})^2/[4 \log (k_{11}k_{22}/Z^2)] \quad (10)$$

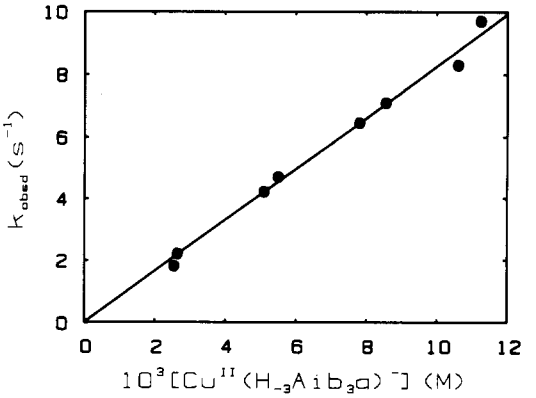

Figure 6. Kinetic data for the electron-transfer reaction of $Ni^{III}(H_{-1}Aib_2)_2^-$ with $Cu^{III}(H_{-3}Aib_3a)^-$ at 25 °C, I = 0.1 ($NaClO_4$), and pH 12–13. The slope corresponds to a cross-exchange rate constant (k_{12}) of 830 M^{-1} s^{-1}.

the copper couple, K_{12} is the equilibrium constant for the cross-exchange reaction, and Z is the bimolecular collision frequency (10^{11} M^{-1} s^{-1}). For $k_{22} = 2.2 \times 10^4$ M^{-1} s^{-1} [42] and K_{12} = 0.26, a value of 1.0×10^2 M^{-1} s^{-1} is obtained for the self-exchange rate constant (k_{11}) of $Ni^{III,II}(H_{-1}Aib_2)_2^{-,2-}$. However, since charged species are involved in the reaction, it is necessary to correct for electrostatic effects:[45]

$$\Delta G_{12}^* = w_{12} + \frac{\Delta G_{11}^* - w_{11} + \Delta G_{22}^* - w_{22} + \Delta G_r°(1 + \alpha)}{2} \quad (11)$$

$$\alpha = \frac{\Delta G_r°}{4(\Delta G_{11}^* - w_{11} + \Delta G_{22}^* - w_{22})} \quad (12)$$

$$\Delta G_r° = \Delta G_{12}° + w_{21} - w_{12} \quad (13)$$

The free energy terms (ΔG^*) were calculated from the experimentally determined rate constants by eq 14. The work terms

$$\Delta G^* = -RT \ln (k/Z) \quad (14)$$

(w) were evaluated according to the Debye–Hückel theory[46] (eq 15) for aqueous solutions at 25 °C and I = 0.1. The approach

$$w = \frac{4.24 z_1 z_2}{\bar{r}(1 + 0.104\bar{r})} \quad (15)$$

distance, $\bar{r}$, is taken as the radii of the two approaching molecules of charges z_1 and z_2. The radii for the Cu(II) and Cu(III) complexes with Aib_3a have been estimated previously as 4.7 and 4.3 Å, respectively.[42] The Ni(II) and Ni(III) radii were estimated from a molecular model based on the X-ray crystal structure for $Ni^{II}(H_{-1}G_2)_2^{2-}$ with appropriate adjustment for the size of Aib.[3] The radii for both complexes (identical ligation) were taken as 4.8 Å. From eq 15, the work terms were calculated as 0.44, 0, 0.22, and 0 for w_{11}, w_{22}, w_{12}, and w_{21}, respectively. The reaction free energy change ($\Delta G_{12}°$) was calculated from the formal electrode potentials as 0.69 kcal. This gives a value of 0.27 kcal for $\Delta G_r°$ and a ΔG_{11}^* value of 12.7 kcal. The corrected self-exchange rate constant for the Ni couple is 48 M^{-1} s^{-1}. This k_{11} value is about 500 times greater than the self-exchange rate constants for $Ni^{III,II}$ (tripeptide) couples, which are approximately 0.1 M^{-1} s^{-1}.[47] The latter value was obtained from cross-reactions with outer-sphere electron-transfer reagents such as $Ru^{II}(NH_3)_5py^{2+}$. The higher k_{11} value for the $Ni^{III,II}(Aib_2)_2$ couple seems to reflect a smaller reorganizational energy involved in the self-exchange reaction for this couple. This is consistent with our proposal that both $Ni^{III}(H_{-2}Aib_2)_2^-$ and $Ni^{II}(H_{-2}Aib_2)_2^{2-}$ are

(42) Anast, J. M.; Hamburg, A. W.; Margerum, D. W. *Inorg. Chem.* **1983**, *22*, 2139–2145.
(43) Nagy, J. C.; Diaddario, L. L.; Margerum, D. W., to be published.
(44) Marcus, R. A. *J. Phys. Chem.* **1963**, *67*, 853–857; *J. Chem. Phys.* **1965**, *43*, 679–701.
(45) Haim, A.; Sutin, N. *Inorg. Chem.* **1976**, *15*, 476–478.
(46) Brown, G. M.; Sutin, N. *J. Am. Chem. Soc.* **1979**, *101*, 883–892.
(47) Kumar, K.; Margerum, D. W., to be submitted for publication.

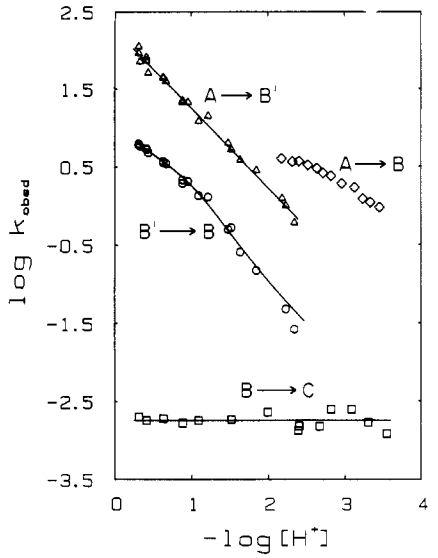

Figure 7. Kinetic data for the acid decomposition of $Ni^{III}(H_{-1}Aib_2)_2^-$ at 25.0 °C and I = 1.0 ($NaClO_4$): (△) $k_{AB'}$ in $HClO_4$ or dichloroacetic acid buffered solutions; (◇) k_{AB} data in chloroacetic acid buffered solution; (○) $k_{B'B}$ and (□) k_{BC}, in $HClO_4$ or dichloroacetic acid buffered solutions.

six-coordinate and have identical ligation. In contrast, Ni^{II}(tripeptide) complexes are square planar whereas the Ni^{III}(tripeptide) complexes are six-coordinate. Water molecules must be added or lost in the self-exchange reaction, which incurs a higher reorganizational energy.

Acid-Catalyzed Dissociation Kinetics. Acid catalyzes the decomposition of tetragonally compressed $Ni^{III}(H_{-1}Aib_2)_2^-$ to give Ni(II), Aib_2, and oxidized peptide fragments. The kinetics of this "self-redox" process were monitored by the loss of Ni(III) absorbance at 410 nm. The kinetic behavior of this system is distressingly complex. In the pH range 0.3–2.4 (perchloric or dichloroacetic acid), the process involves three sequential reactions. In chloroacetic acid medium (pH 2.1–3.6), the decomposition of $Ni^{III}(H_{-1}Aib_2)_2^-$ involves two sequential reactions that include a general-acid-catalyzed step. In all cases, kinetics were measured under pseudo-first-order conditions with acid in excess. The ratios of sequential first-order rate constants were sufficiently large to permit their individual resolution by multiple linear-regression analysis. log k_{obsd} values for the pseudo-first-order rate constants are plotted as a function of pH in Figure 7 for each of the steps. The intermediates are characterized by EPR spectroscopy, and mechanistic details are proposed to explain some of the observed acid dependencies.

In perchloric or dichloroacetic acid solution (pH 0.3–2.4), the tetragonally compressed $Ni^{III}(H_{-1}Aib_2)_2^-$ complex (A) decomposes to give Ni(II) plus peptide and oxidation products (C) in a three-reaction sequence (eq 16). The first two reactions are

$$A \xrightarrow{k_{AB'}} B' \xrightarrow{k_{B'B}} B \xrightarrow{k_{BC}} C \qquad (16)$$

acid-catalyzed, and the rate of the third reaction is independent of acid concentration. Absorbance decreases are about 5, 45, and 50% of the total initial absorbance at 410 nm for the A → B', B' → B, and B → C reactions, respectively. Kinetics data for the decomposition of $Ni^{III}(H_{-1}Aib_2)_2^-$ in this pH range are given in Table IV. Intermediates B' and B are EPR active, and the EPR spectra are shown in Figure 8. The calculated EPR parameters for species B' and B are given in Table II. These signals have $g_\perp > g_\parallel$, which is indicative of a tetragonally elongated octahedral arrangement. The lack of splitting in the $g_\parallel$ region indicates that the nitrogens (nuclear spin = 1) are not coordinated axially. Scheme III shows proposed structures for these intermediates that are consistent with the observed EPR spectra.

The reaction of Ni(III) with iodide to produce triiodide (I_3^-) was used to quantitate the amount of Ni(III) present during the acid decomposition of $Ni^{III}(H_{-1}Aib_2)_2^-$. This analysis shows that no Ni(III) is lost before the B → C reaction occurs. Since the same amount of Ni(III) is present in species A and B, this eliminates the possibility that species B' yields Ni(II) directly.

Table IV. Kinetic Data for the Decomposition of $Ni^{III}(H_{-1}Aib_2)_2^-$ at pH 0.3–2.4 in Perchloric or Dichloroacetic Acid[a]

[H+], M	$k_{AB'}$, s^{-1}	$k_{B'B}$, s^{-1}	$10^3 k_{BC}$, s^{-1}	ref
4.8×10^{-1}	$(1.1 \pm 0.3) \times 10^2$	6.1 ± 0.1	2.0 ± 0.1	*b*
4.8×10^{-1}	$(9.0 \pm 0.2) \times 10$	5.9 ± 0.5		*c*
4.6×10^{-1}	$(7.0 \pm 1.0) \times 10$	5.7 ± 0.3		*d*
3.8×10^{-1}	$(8.0 \pm 2.0) \times 10$	5.3 ± 0.1	1.8 ± 0.1	*b*
3.8×10^{-1}	$(7.2 \pm 0.7) \times 10$	5.2 ± 0.2		*c*
3.6×10^{-1}	$(5.0 \pm 1.0) \times 10$	4.7 ± 0.3		*d*
2.3×10^{-1}	$(4.4 \pm 0.8) \times 10$	3.5 ± 0.1	1.9 ± 0.1	*b*
2.3×10^{-1}	$(4.3 \pm 0.5) \times 10$	3.63 ± 0.05		*c*
2.1×10^{-1}	$(3.9 \pm 0.6) \times 10$	3.4×0.1		*d*
1.3×10^{-1}	$(2.2 \pm 0.2) \times 10$	1.9 ± 0.2	1.67 ± 0.08	*b*
1.3×10^{-1}	$(2.1 \pm 0.2) \times 10$	2.1 ± 0.1		*c*
1.1×10^{-1}	$(2.1 \pm 0.1) \times 10$	2.02 ± 0.1		*d*
8.0×10^{-2}	$(1.2 \pm 0.1) \times 10$	1.32×0.04	1.80 ± 0.05	*b*
6.0×10^{-2}	$(1.4 \pm 0.2) \times 10$	1.27 ± 0.05		*d*
3.3×10^{-2}	6.3 ± 0.5	$(4.93 \pm 0.06) \times 10^{-1}$		*e*
3.0×10^{-2}	5.2 ± 0.5	$(5.2 \pm 0.4) \times 10^{-1}$	1.85 ± 0.06	*b*
2.3×10^{-2}	3.8 ± 0.3	$(2.52 \pm 0.03) \times 10^{-1}$		*e*
1.4×10^{-2}	2.8 ± 0.2	$(1.47 \pm 0.04) \times 10^{-1}$		*e*
1.0×10^{-2}			2.3 ± 0.2	*b*
6.5×10^{-3}	1.23 ± 0.01			*e*
5.8×10^{-3}	$(9.9 \pm 0.7) \times 10^{-1}$	$(4.7 \pm 0.1) \times 10^{-2}$		*e*
4.5×10^{-3}	$(6.0 \pm 0.1) \times 10^{-1}$	$(2.6 \pm 0.2) \times 10^{-2}$		*e*

[a] 25.0 °C, I = 1.0 ($NaClO_4$). All rate constants are the average of at least three trials; uncertainties are one standard deviation. [b] 10-fold excess of Aib_2; [Ni(III)] = 2.0×10^{-4} M. [c] 10-fold excess of Aib_2; [Ni(III)] = 4.1×10^{-4} M. [d] 20-fold excess of Aib_2; [Ni(III)] = 2.0×10^{-4} M. [e] 10-fold excess of Aib_2; [Ni(III)] = 2.0×10^{-4} M; 0.1 M dichloroacetic acid as a buffer.

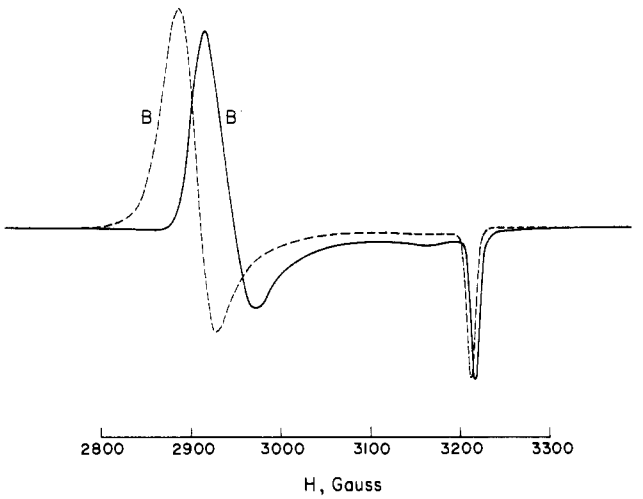

Figure 8. EPR spectra for $Ni^{III}(H_{-1}Aib_2)_2^-$ acid decomposition intermediates B'(—) at pH 7.5 and B (- -) at pH 1.5, −150 °C, and I = 1.0 ($NaClO_4$).

Interestingly, species B' can also be generated by bulk electrolysis of the $Ni^{II}(Aib_2)_2$ complex at pH 8 (primarily $Ni^{II}(Aib_2)_2$). The yield of Ni(III) for this process is about 10% at pH 7.5. Upon standing at room temperature for several minutes at pH 7.5, species B' will rearrange to give species A (tetragonally compressed). Alternatively, addition of acid to species B' gives species B. Thus, at pH 7.5 the A → B' reaction is reversible. However, this reaction is not reversible under the conditions used for the acid decomposition kinetics analysis (pH 0.3–2.4).

Pseudo-first-order rate constants ($k_{AB'}$) for the A → B' reaction (perchloric or dichloroacetic acid solution) follow a simple first-order dependence on [H+] (Figure 7) and give a second-order rate constant of 187 ± 6 M^{-1} s^{-1}. Data for the B' - B reaction ($k_{B'B}$) show a complicated dependence on [H+].

The nonlinear variation of $k_{B'B}$ with [H+] is evident in the plot in Figure 9. At very low [H+], the data show slightly less than a first-order dependence in [H+]. At greater acid concentrations, the order in [H+] increases to ≃1.5 followed by a decrease to ≃0.8 order at high [H+]. A complicated dependence on [H+] for the

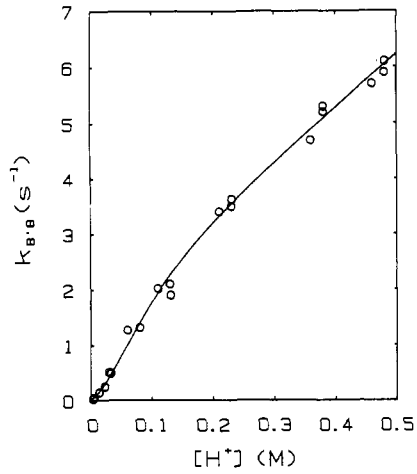

Figure 9. Acid decomposition rate constants for $Ni^{III}(H_{-1}Aib_2)_2^-$: $k_{B'B}$ data, 25.0 °C. The solid line is calculated from eq 20 with $k_1 = 1.7\ s^{-1}$, $k_{-1}/k_2 = 0.010$, and $k_3 = 9.3\ M^{-1}\ s^{-1}$.

B′ → B reaction is consistent with the proposed structures for B′ and B in Scheme III. At least two protonations (of the terminal carboxylate groups coordinated to Ni^{III}) must occur for the rearrangement to take place. The mechanism proposed to account for the observed acid dependence is given in eq 17–19. The

$$B' \underset{k_{-1}}{\overset{k_1}{\rightleftharpoons}} B'' \tag{17}$$

$$B'' + 2H^+ \xrightarrow{k_2} B + H^+ \tag{18}$$

$$B' + H^+ \xrightarrow{k_3} B \tag{19}$$

observed pseudo-first-order rate constant ($k_{B'B}$) with B″ as a steady state intermediate is given by eq 20.

$$k_{B'B} = \frac{k_1 k_2 [H^+]^2}{k_{-1} + k_2[H^+]^2} + k_3[H^+] \tag{20}$$

This mechanism requires an acid-independent rearrangement of B′ to give species B″ (eq 17). This species is a steady-state intermediate and can react with two protons to give the product, B, as in eq 18. Alternatively, B′ can react directly with a proton to give B (eq 19). The solid line in Figure 9 gives the calculated fit of eq 20 to the experimental rate data with $k_1 = 1.7\ (2)\ s^{-1}$, $k_{-1}/k_2 = 0.010\ (9)$, and $k_3 = 9.3\ (5)\ M^{-1}\ s^{-1}$ (digits in parentheses are estimated standard deviations in the last digit).

The third reaction in the decomposition sequence in the pH range 0.3–2.4 is the redox step, B → C, in which the elongated Ni(III) intermediate, B, is reduced to Ni(II) at the expense of Aib_2 oxidation. This reaction is independent of [H^+] (Figure 7).

The decomposition of $Ni^{III}(H_{-1}Aib_2)_2^-$ at pH 2.1–3.6 with chloroacetic acid as the buffer involves only two sequential reactions. The EPR spectrum of the intermediate for this process corresponds to species B in eq 16. In addition, the absorbance change corresponds to A → B in Scheme III. Thus, at pH 2.1–3.6 in chloroacetic acid solution, only the A → B and B → C reactions occur. No species B′ is observed. The kinetics data for the two sequential reactions observed in this pH range in chloroacetic acid are given in Table V. Table V also includes kinetics data collected at various chloroacetic acid buffer concentrations. It was observed that the k_{AB} values are dependent on the concentration of the buffer. For example, at $[H^+] = 1.4 \times 10^{-3}$ M and $[X]_T = 0.05$, 0.15, or 0.20 M (where $[X]_T = [HX] + [X^-]$), observed pseudo-first-order rate constants (k_{AB}) are 1.28, 3.2, and 3.8 s^{-1}, respectively. Clearly, chloroacetic acid catalyzes the A → B reaction. The observed rate constant for a reaction having a first-order dependence on [H^+] as well as a first-order dependence on the concentration of a general acid, [HX], can be expressed by eq 21, where k_H is the second-order rate constant for the path

$$k_{obsd} = k_H[H^+] + k_{HX}[HX] \tag{21}$$

Table V. Kinetic Data for the Decomposition of $Ni^{III}(H_{-1}Aib_2)_2^-$ at pH 2.1–3.6 in Chloroacetic Acid[a]

$[H^+]$, M	$[X]_T$, M	k_{AB}, s^{-1}	$10^3 k_{BC}$, s^{-1}
3.5×10^{-3}	5.0×10^{-2}	1.78 ± 0.07	
1.4×10^{-3}	5.0×10^{-2}	1.28 ± 0.02	
6.6×10^{-3}	1.0×10^{-1}	4.0 ± 0.1	
4.8×10^{-3}	1.0×10^{-1}	3.64 ± 0.07	
4.0×10^{-3}	1.0×10^{-1}		1.34 ± 0.05
3.9×10^{-3}	1.0×10^{-1}	3.7 ± 0.1	1.53 ± 0.06
3.0×10^{-3}	1.0×10^{-1}	3.31 ± 0.04	
2.3×10^{-3}	1.0×10^{-1}	3.0 ± 0.2	
2.1×10^{-3}	1.0×10^{-1}		1.51 ± 0.05
1.9×10^{-3}	1.0×10^{-1}	2.6 ± 0.1	
1.5×10^{-3}	1.0×10^{-1}	2.4 ± 0.1	2.5 ± 0.3
1.1×10^{-3}	1.0×10^{-1}	1.92 ± 0.08	
8.1×10^{-4}	1.0×10^{-1}		2.5 ± 0.3
7.4×10^{-4}	1.0×10^{-1}	1.7 ± 0.2	
5.8×10^{-4}	1.0×10^{-1}	1.22 ± 0.06	
4.9×10^{-4}	1.0×10^{-1}		1.7 ± 0.1
4.6×10^{-4}	1.0×10^{-1}	1.1 ± 0.1	
3.5×10^{-4}	1.0×10^{-1}	0.95 ± 0.04	
2.8×10^{-4}	1.0×10^{-1}		1.22 ± 0.01
1.6×10^{-3}	1.5×10^{-1}	2.79 ± 0.05	
1.4×10^{-3}	1.5×10^{-1}	3.2 ± 0.2	
1.4×10^{-3}	2.0×10^{-1}	3.8 ± 0.2	
7.8×10^{-4}	2.0×10^{-1}	3.2 ± 0.2	

[a] 25.0 °C, $I = 1.0$ ($NaClO_4$), $[X]_T = [HX] + [X^-]$ where HX = chloroacetic acid and X^- = chloroacetate. All rate constants are the average of at least three trials; uncertainties are 1 standard deviation.

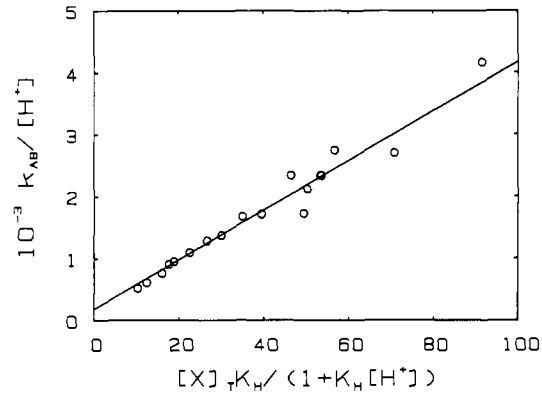

Figure 10. Dependence of k_{AB} (defined in Scheme III) on chloroacetic acid and [H^+] concentration at 25.0 °C. The plot is a fit of eq 22.

proceeding by proton transfer from H_3O^+ and k_{HX} is the second-order rate constant for proton transfer from HX. The relationship between k_{obsd} and the total buffer concentration, $[X]_T$, and the protonation constant for the general acid, K_H, is given in eq 22.

$$\frac{k_{obsd}}{[H^+]} = k_H + \frac{k_{HX}[X]_T K_H}{1 + K_H[H^+]} \tag{22}$$

The calculated $k_{AB}/[H^+]$ vs $[X]_T K_H/(1 + K_H[H^+])$ data for the A → B reaction are plotted in Figure 10. The solid line has been forced through a y intercept of 187 $M^{-1}\ s^{-1}$, which is the k_H value for the disappearance of species A obtained for the A → B′ reaction. Since both reactions (A → B′ and A → B) follow the disappearance of A, the second-order k_H rate constant is the same for each. The slope of the line in Figure 10 gives a k_{HX} value of 40 $M^{-1}\ s^{-1}$. The explanation for the general-acid catalysis of this reaction is that the rate-determining step involves "inside protonation" of a peptide nitrogen that occurs simultaneously with the breaking of a metal–peptide bond. This type of reaction has previously been shown to be general-acid catalyzed.[48] In this case, the cleavage of the Ni–N(peptido) bond weakens the Ni–N(amino) and Ni–O(carboxyl) bonds of the same dipeptide chain. This

(48) Youngblood, M. P.; Chellappa, K. L.; Bannister, C. E.; Margerum, D. W. *Inorg. Chem.* **1981**, *20*, 1742–1747.

Table VI. Rate Constants for the Self-Redox Reactions (B → C) of Ni(III) Bis(dipeptido) Complexes[a]

dipeptide	k_{BC}, s^{-1}	ref	dipeptide	k_{BC}, s^{-1}	ref
GG	0.15 ± 0.01	*b*	GA	0.029 ± 0.004	*b*
AG	0.084 ± 0.006	*b*	AA	0.016 ± 0.006	*b*
AibG	0.079 ± 0.002		Aib_2	0.0018 ± 0.0004	*c*

[a] 25.0 °C. [b] Reference 4; I = 0.1–0.5. [c] This work; I = 1.0.

allows the rearrangement to take place followed by re-formation of the Ni–N(peptido) bond.

The second reaction in the two-reaction decomposition of $Ni^{III}(H_{-1}Aib_2)_2^-$ in chloroacetic acid (pH 2.1–3.6) is the self-redox step, B → C. This reaction is independent of $[H^+]$ and [HX], so that the reaction rate in chloroacetic acid is the same as in perchloric acid and dichloroacetic acid (pH 0.3–2.4), as seen in Figure 7. The value of k_{BC} is (1.83 ± 0.04) × 10^{-3} s^{-1} for the pH range 0.3–3.6. Table VI shows a comparison of this reaction rate with the rates of self-redox for other Ni(III) bis(dipeptido) complexes, which correspond to the acid-independent conversion of B to C in Scheme I. The value of k_{BC} for $Ni^{III}(H_{-1}Aib_2)_2^-$ is about 100 times slower than that for $Ni^{III}(H_{-1}G_2)_2^-$. This reflects the stabilization to Ni(III) by Aib peptides relative to acid-catalyzed self-redox reactions.

Direct comparison can be made for the decomposition rate of $Ni^{III}(H_{-1}Aib_2)_2^-$ versus other bis(dipeptido)nickel(III) complexes for the reactions prior to the self-redox step. The A → B′ reaction was not found for $Ni^{III}(H_{-1}G_2)_2^-$ and other dipeptides.[4] The reaction has a small absorbance change and is quite rapid so that it could not be observed by stopped-flow spectroscopy. Therefore, the B′ - B reaction for the $(Aib_2)_2$ complex is comparable to the A → B reaction for the other bis(dipeptido)nickel(III) complexes. The B′ - B reaction for $Ni^{III}(H_{-1}Aib_2)_2^-$ has a complicated acid dependence, but a second-order rate constant of approximately 13 M^{-1} s^{-1} can be estimated by linear regression analysis of the data in Figure 9. This is much slower than the second-order rate constant for the A → B reaction of $Ni^{III}(H_{-1}G_2)_2^-$ (105 ± 3) and is comparable to those for $Ni^{III}(H_{-1}GA)_2^-$ and $Ni^{III}(H_{-1}AA)_2^-$, which are 12 ± 1 and 5.5 ± 0.7 M^{-1} s^{-1}, respectively.[4] The conversion of A to B for these systems was not observed to be general-acid catalyzed, even for the pH range where chloroacetic acid was used as a buffer. However, the maximum buffer concentration in those studies was 0.01 M. In the present work, at least 0.1 M buffer was used. This may explain the lack of general-acid effect in the previous studies. In addition, the previous studies showed only a single reaction (A → C) above pH 2. In the case of $Ni^{III}(H_{-1}Aib_2)_2^-$, however, two reactions are observed even at pH 3.6, because species B is also stabilized by increased *C*-methyl substitution.

Conclusions

The effect that replacement of G residues by Aib residues has on the stability and electrode potential of metal peptide complexes varies greatly with the nature of the complex. Thus, the stability constant of $Ni^{II}(H_{-2}Aib_3)^-$ is increased by a factor of $10^{3.2}$ compared to that of $Ni^{II}(H_{-2}G_3)^-$,[49] whereas the stability constant of $Ni^{II}(H_{-1}Aib_2)_2^{2-}$ is decreased by a factor of $10^{1.88}$ compared to that of $Ni^{II}(H_{-1}G_2)_2^{2-}$. The latter decrease occurs despite the fact that the increase in donor strength for Aib_2 causes spin pairing in the $Ni^{II}(H_{-1}Aib_2)_2^{2-}$ complex. Some other effect, probably changes of solvation of the complexes, decreases the stability constants as alkyl groups replace hydrogens in the dipeptide complexes (Table I).

There is little difference in the electrode potentials for $Ni^{III,II}(H_{-2}Aib_3)^{0,-}$ ($E°$ = 0.83 V)[14] compared to $Ni^{III,II}(H_{-2}G_3)^{0,-}$ ($E°$ = 0.85 V).[13] On the other hand, there is a large change in the $E°$ values for $Ni^{III,II}(H_{-1}Aib_2)_2^{-,2-}$ (0.34 V) compared to $Ni^{III,II}(H_{-1}G_2)_2^{-,2-}$ (0.66 V). The $Cu^{II}(H_{-2}Aib_3)^-$ complex is $10^{1.8}$ times more stable than the $Cu^{II}(H_{-2}G_3)^-$ complex.[18] The $Cu^{III,II}(H_{-2}Aib_3)^{0,-}$ $E°$ value is 0.66 V[22] compared to an $E°$ value of 0.92 V for the $Cu^{III,II}(H_{-2}G_3)^{0,-}$ couple.[50] The tripeptide complexes of Ni(II) and Cu(III) have a square-planar geometry, while the tripeptide complexes of Ni(III) and Cu(II) have tetragonally elongated six-coordinate geometries with water in the axial positions. By contrast, the Ni(III) and Ni(II) bis(dipeptido) complexes have tetragonally compressed six-coordinate geometries. The redox potential for $Ni^{III,II}(H_{-1}Aib_2)_2^{-,2-}$, 0.34 V, is much closer to the Ni(III,II) potentials reported for systems of biological interest.

Acknowledgment. This investigation was supported by Public Health Service Grant No. GM12152 from the National Institute of General Medical Sciences. The assistance of B. E. Schwederski with the NMR studies is greatly appreciated.

(49) Kennedy, W. R.; Margerum, D. W. *Inorg. Chem.* **1985**, *24*, 2490–2495.
(50) Bossu, F. P.; Chellappa, K. L.; Margerum, D. W. *J. Am. Chem. Soc.* **1977**, *99*, 2195–2203.